



HAL
open science

Proximity-Effect Driven Reversibility in Superconducting Constrictions

Nikhil Kumar, Thierry Fournier, Hervé Courtois, Clemens Winkelmann, A. K.
Gupta

► **To cite this version:**

Nikhil Kumar, Thierry Fournier, Hervé Courtois, Clemens Winkelmann, A. K. Gupta. Proximity-Effect Driven Reversibility in Superconducting Constrictions. 2014. hal-01090069

HAL Id: hal-01090069

<https://hal.science/hal-01090069>

Preprint submitted on 2 Dec 2014

HAL is a multi-disciplinary open access archive for the deposit and dissemination of scientific research documents, whether they are published or not. The documents may come from teaching and research institutions in France or abroad, or from public or private research centers.

L'archive ouverte pluridisciplinaire **HAL**, est destinée au dépôt et à la diffusion de documents scientifiques de niveau recherche, publiés ou non, émanant des établissements d'enseignement et de recherche français ou étrangers, des laboratoires publics ou privés.

Proximity-Effect Driven Reversibility in Superconducting Constrictions

Nikhil Kumar,¹ T. Fournier,^{2,3} H. Courtois,^{2,3} C. B. Winkelmann,^{2,3} and Anjan K. Gupta¹

¹*Department of Physics, Indian Institute of Technology Kanpur, Kanpur 208016, India*

²*Université Grenoble Alpes, Institut Néel, F-38042 Grenoble, France*

³*CNRS, Institut Néel, F-38042 Grenoble, France*

(Dated: November 27, 2014)

We demonstrate the role of proximity effect in the thermal hysteresis of superconducting constrictions. From the analysis of successive thermal instabilities in the transport characteristics of micron-size superconducting quantum interference devices with a well-controlled geometry, we obtain a complete picture of the different thermal regimes. These determine whether the junctions are hysteretic or not. Below the superconductor critical temperature, the critical current switches from a classical weak-link behavior to one driven by the proximity effect. The associated small amplitude of the critical current makes it robust with respect to the heat generation by phase-slips, leading to a non-hysteretic behavior.

Micron-size superconducting quantum interference devices (μ -SQUID), consisting of two parallel weak links (WLs) acting as Josephson junctions in a small superconducting (SC) loop, have been of interest for probing magnetism at small scales [1–4]. One of the major obstacles of a μ -SQUID proper operation is its hysteretic (or bistable) current-voltage characteristic (IVC). When the current is ramped up, it switches to a dissipative state at the critical current I_c . When the current is ramped down from above I_c , it comes back to a zero-voltage state at a smaller current, called the re-trapping current I_r . In conventional tunnel-barrier type Josephson-junctions, the hysteresis arises from large junction capacitance [5]. In WLs or μ -SQUIDS, with negligible capacitance, hysteresis is found at low temperatures below a crossover temperature $T_h < T_c$ [6], with T_c as the SC critical temperature. Although it has been claimed that an effective capacitance can arise from the recovery time of the SC order parameter [7], it is now understood that hysteresis in WLs is of thermal origin [9–11], similar to that observed in superconductor-normal metal-superconductor junctions [8]. Thermal hysteresis in SC-WLs and how it affects the IVCs can be modeled by considering local thermal balance which dictates the position of the normal metal-superconductor (N-S) interface [9–11]. In case of poor heat evacuation, phase fluctuations can trigger a thermal run-away giving a large resistive hot-spot. This topic is of great practical importance, in particular for SC-magnet wires and cables, helium level sensors, bolometers [12], μ -SQUIDS and other nano-scale SC structures [13]. A systematic understanding of various thermal phases which a typical device exhibits is much desired, in particular to make devices with intrinsic non-hysteretic behavior.

In this Letter, we report on the transport characteristics of Nb-film based μ -SQUIDS with a well-controlled geometry and describe a complete picture of different thermal regimes. The IVCs show a critical current and two re-trapping currents that we describe using a thermal instability model in SC leads. The critical current

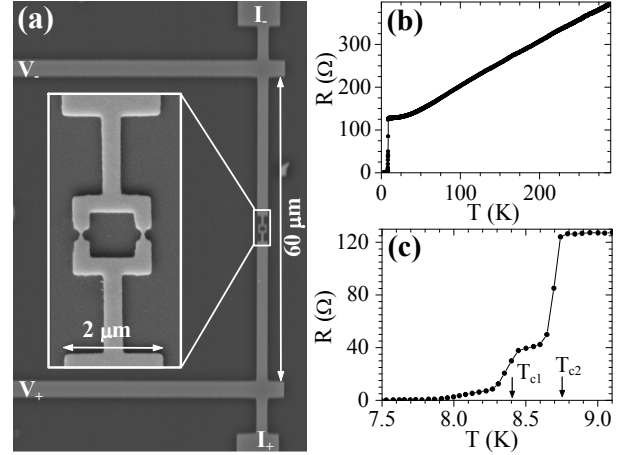


FIG. 1: (a) SEM image of the μ -SQUID μ S1 with its current and voltage leads. The zoomed-in image shows the SQUID loop (with area $1 \times 1 \mu\text{m}^2$) and the narrow leads. (b) Resistance vs temperature (R-T) plot. (c) Low-temperature portion of the R-T plot, showing multiple transitions, for μ S1 at a bias current of 0.01 mA.

I_c follows the theoretical expectation at low temperature but changes its behavior while crossing the smaller re-trapping current. In this hysteresis-free regime, the WLs superconduct, despite being slightly heated by individual phase slips, thanks to the proximity effect of the adjacent superconductor.

We fabricated μ -SQUIDS from Nb films using common techniques [2, 14–16]. After cleaning the Si substrate with an oxygen plasma, we deposited a 31 nm thick Nb film using e-beam evaporation in a UHV system. We then patterned the structures with electron beam lithography followed by deposition of a 20 nm thick Al film. A lift-off then transferred the pattern to the Al film, which acts as a mask during the reactive ion etching of Nb using SF_6 plasma. Finally, the Al film was removed chemically. The transport measurements were carried out down to a temperature of 4.2 K in a home-made liquid helium dip-

per cryostat with built-in copper-powder filters [6]. We have studied more than four devices with similar behavior, but here we report on two typical devices denoted by μ S1 and μ S2.

For all devices, the patterned SQUID-loop area is $1 \mu\text{m}^2$ and the width of its arms is $0.3 \mu\text{m}$. The designed WL length is 150 nm while the WL width is 70 and 50 nm in μ S1 and μ S2, respectively. Fig. 1(a) shows the SEM image of the device μ S1. The pattern includes four different parts contributing to the electrical characteristics. The first part is the two WLs, each of normal resistance R_{WL} . The second one is the SQUID loop with normal resistance as R_L including the resistance of the parallel WLs. The third part comprises the narrow leads of width $0.3 \mu\text{m}$ and length $1.7 \mu\text{m}$ on either side of the SQUID loop, each with a resistance R_1 . Finally, each narrow lead meets a wider lead of width $2 \mu\text{m}$, length $27.5 \mu\text{m}$ and normal resistance R_2 . From the geometry, various resistances can be expressed in terms of the films's square resistance R_\square so that the total normal-state resistance between the voltage leads is $R_N = R_L + 2R_1 + 2R_2 = 40.3R_\square + 0.5R_{WL}$.

Figure 1(b) and (c) show temperature dependence of the four-probe resistance R for μ S1. Multiple superconducting transitions are observed. The resistance jumps from its residual value 128Ω down to about 40Ω at $T_{c2} = 8.7 \text{ K}$, jumps further down from 38 to 8Ω at $T_{c1} = 8.35 \text{ K}$, and finally decreases smoothly to zero. We attribute the first transition at T_{c2} to the wide leads, the second one at T_{c1} to both the narrow leads and the SQUID loop. From IVC in non-hysteretic regime, discussed later [see Fig. 3(f)], we deduce $R_{WL} \simeq 8 \Omega$. This analysis is consistent with $R_\square = 3.1 \Omega$, giving a resistivity of $9.5 \mu\Omega\cdot\text{cm}$.

Next we discuss a one-dimensional model of thermal instability in long current-biased SC leads. This is similar to Broom and Rhoderick [17] model, which analyzes the dynamics of an N-S interface under the influence of an electrical current. Thus a critical magnitude of current is found at which the N-S interface changes its direction of motion. Here we consider a SC lead with normal state resistivity ρ_n , uniform thickness t and width w , and carrying an electrical current I as shown in Fig. 2(a). The heat transfer with the substrate at a bath temperature T_b writes $\alpha(T - T_b)/t$, where the coefficient α is characteristic of the interface. The thermal conductivity κ is constant and uniform. An N-S interface exists at $x = 0$, so that the temperature T is equal to T_c at this point. A heat current flows from $x < 0$ due to the resistance of this lead portion plus possibly a device at the end of the lead. With the boundary condition $T = T_b$ at $x \rightarrow \infty$, the heat equation solution in the SC portion of the lead is $T = T_b + (T_c - T_b)\exp(-x/l_{th})$. The thermal healing length $l_{th} (= \sqrt{\kappa t/\alpha})$ is a crossover length-scale such that for $\Delta x \gg l_{th}$ substrate heat-loss dominates and for $\Delta x \ll l_{th}$ conduction dominates. The heat current at the N-S interface ($x = 0$) is then $\dot{Q}_0 = w\alpha l_{th}(T_c - T_b)$, which

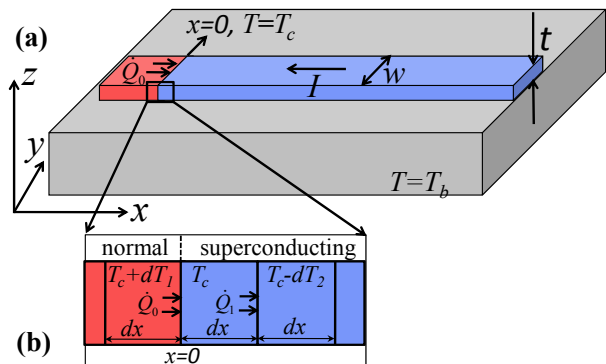


FIG. 2: (a) Schematic of the semi-infinite (in $+x$ direction) lead of SC material on a substrate at bath temperature T_b with N-S interface at $x = 0$. (b) shows the region near the N-S interface with three differential elements of length dx when the N-S interface stabilizes near the heat source on left.

implies an effective thermal resistance of $(w\alpha l_{th})^{-1}$ as seen from the N-S interface. It is important to realize that the N-S interface will shift to the right (left) if more (less) than \dot{Q}_0 heat is incident on the lead at $x = 0$.

For analyzing the stability of the N-S interface, we look into the effect of fluctuations on a differential element (from $x = 0$ to $x = dx$) at this interface in a quasi-static approximation. If this element turns resistive, see Fig. 2(b), an additional power $I^2 \rho_n dx / (wt)$ is generated. This extra heat is shared equally between the left and right interfaces to the lead, while the substrate receives a negligible amount [18]. The heat current across the new N-S interface is $\dot{Q}'_1 = \dot{Q}_0 - \alpha(T_c - T_b)w dx + I^2 \rho_n dx / (2wt)$. As pointed out before, if this heat is more (less) than \dot{Q}_0 , the N-S interface will shift to the right (left) implying instability (stability). Thus the maximum current that the lead can carry without causing a thermal instability is given by $\alpha(T_c - T_b)w dx = I_{max}^2 \rho_n dx / (2wt)$ or

$$I_{max} = w \sqrt{2\alpha(T_c - T_b)/R_\square}. \quad (1)$$

This expression is consistent with Ref. [9] results in the limiting case of a very long SC lead and equal thermal conductivities of SC and normal metal, which is valid close to the N-S interface. In this model, the lead needs to be much longer than l_{th} so that the overall thermal resistance as seen from the N-S interface does not depend on its position. When I exceeds I_{max} , the N-S interface will runaway to a large x location where the lead joins a thermal bath (or a much wider lead) as the thermal resistance to the thermal bath will be less there. By analyzing the stability of a small resistive element against an incursion to the SC state, one finds as expected the same expression for the re-trapping current. It would be more appropriate to call I_{max} as the ‘instability current’ as it describes both the runaway and re-trapping of the N-S interface. We will use the term ‘re-trapping’ current,

as it has been done in most earlier works.

In order to quantify in our case the relevant parameters, we use the Wiedemann-Franz law to estimate the thermal conductivity as $\kappa = LT/\rho$ with $L = 2.44 \times 10^{-8} \text{ W}\cdot\Omega/\text{K}^2$ as the Lorenz number. Using $T = T_c = 8.5 \text{ K}$ and $\rho = 9.5 \mu\Omega\cdot\text{cm}$, we get $\kappa = 2.4 \text{ W}/\text{cm}\cdot\text{K}$. Typical values of α that have been used in literature [9, 11] range in 1 to 10 $\text{W}/\text{cm}^2\cdot\text{K}$. We use $\alpha = 5.3 \text{ W}/\text{cm}^2\cdot\text{K}$ as found from the temperature dependence of a re-trapping current as discussed later. From these values, we estimate the thermal healing length for our devices as $l_{th} = 1.6 \mu\text{m}$. The length of the wide leads, i.e. $27.5 \mu\text{m}$, is thus much longer than l_{th} while that of the narrow leads, i.e. $1.7 \mu\text{m}$, is only comparable to l_{th} .

Fig. 3 shows IVCs of μS1 , depicting sharp jumps in voltage at three different currents, namely I_{r1} , I_{r2} and I_c . The critical current I_c is defined by the first jump seen while ramping the current up from zero. It shows a distribution of values with, for μS1 , a width of about $40 \mu\text{A}$ for a mean value of 1.3 mA at 4.2 K [18]. From the IVC slope, the resistance just above I_{r1} is about 48Ω . This value is close to the sum $R_L + 2R_1 = 40 \Omega$ of the resistances of the SQUID loop and the narrow leads, which means that the latter are heated to above T_c for $I > I_{r1}$. The observed extra resistance indicates that a portion of the wide leads is also heated to above T_c , thus contributing to the resistance. The second re-trapping current I_{r2} arises from a thermal instability in the long and wide leads. The IVC slope above I_{r2} is 140Ω , which is close to the normal-state resistance value 128Ω , indicating a thermal runaway till the voltage leads. The slightly larger value seen here is due to the heating in the central portion to more than 50 K as estimated from a thermal model. At higher temperatures when I_{r2} is much less and thus the heating is also reduced, the resistance above I_{r2} is found to be exactly 128Ω . In this regime, Fig. 3(f) shows that the resistance just above I_c is about 4Ω from which we deduce R_{WL} as 8Ω . Only the critical current I_c was found to oscillate with the magnetic flux [18] as expected for a SQUID. The retrapping currents $I_{r1,2}$ do not, which confirms that they are not dependent on the SC of the WL.

The three currents I_{r1} , I_{r2} and I_c evolve differently with temperature. Near 5.7 K , I_c crosses I_{r2} [see Fig. 3(b)] and at $T = T_h = 7.25 \text{ K}$, I_c crosses I_{r1} [see Fig. 3(e)], so that hysteresis is absent at higher temperature [see Fig. 3(f)]. We observe sharp voltage changes corresponding to the three currents, making them distinguishable from each other. With increasing temperature, while the IVC near I_c becomes relatively smooth, the voltage jump corresponding to I_{r1} remains sharp and evolves over this smooth feature. Also, the hysteresis does not disappear until I_{r1} fully crosses this smooth feature [see Fig. 3(e)]. This confirms that the two transitions have distinct origins.

Figure 4(a) summarizes the bath-temperature depen-

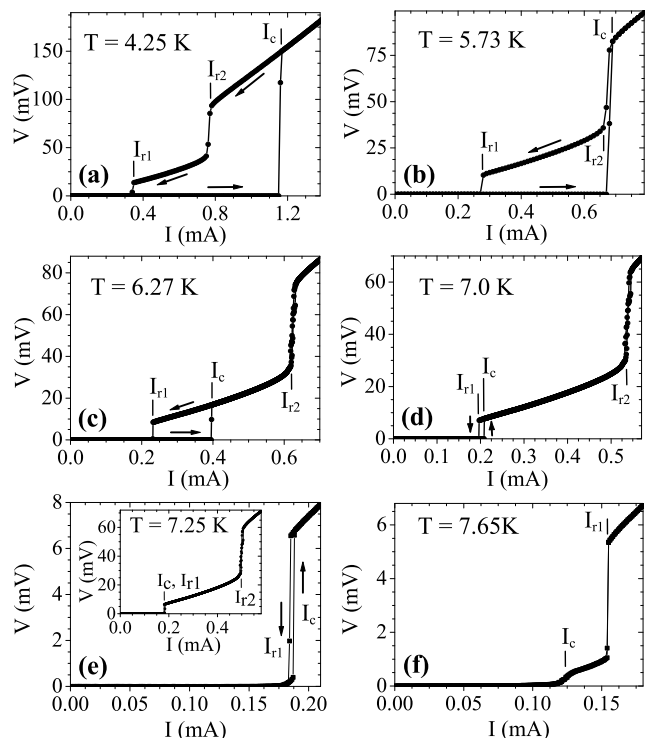


FIG. 3: (a) - (d) IVCs in hysteretic regime for μS1 at different temperatures. A large hysteresis is seen at 4.25 K with two re-trapping currents, I_{r1} and I_{r2} . I_c crosses I_{r2} near 5.7 K and I_{r1} around 7.25 K as seen in (e). (f) shows the IVC of μS1 in the non-hysteretic regime above $T_h = 7.25 \text{ K}$. The inset of (e) shows a larger bias-current range plot to show the I_{r2} transition.

dence of I_c , I_{r1} and I_{r2} for μS1 . Fig. 4(b) shows the same for the device μS2 , which has narrower WLs as compared to μS1 , leading to a smaller critical current, and thus a smaller crossover temperature and a wider temperature range of non-hysteretic IVCs. The retrapping currents $I_{r1,2}$ are the same in the two samples, which confirms that these are independent of the WL structure. With increasing bath temperature, the critical current I_c decreases linearly in both devices up to T_h , where it shows a marked change in behavior. For both devices, I_c and I_{r1} go to zero at the temperature T_{c1} , while I_{r2} vanishes at T_{c2} . This is consistent with the R-T behavior of Fig. 1(c) for μS1 . In both plots, we also indicate the state (resistive or SC) of different portions of the device when the current is ramped down, which constitutes a kind of a phase diagram, or more appropriately, state diagram. The light gray-shaded area shows the bistable region where the whole device is in the fully SC state during the current ramp-up from zero. In the dark gray-shaded region, only the WLs are resistive. No hysteresis is observed in the related temperature range $[T_h, T_{c1}]$. This is the most desirable mode for a SQUID, but it occurs in quite a limited temperature window. At a fixed

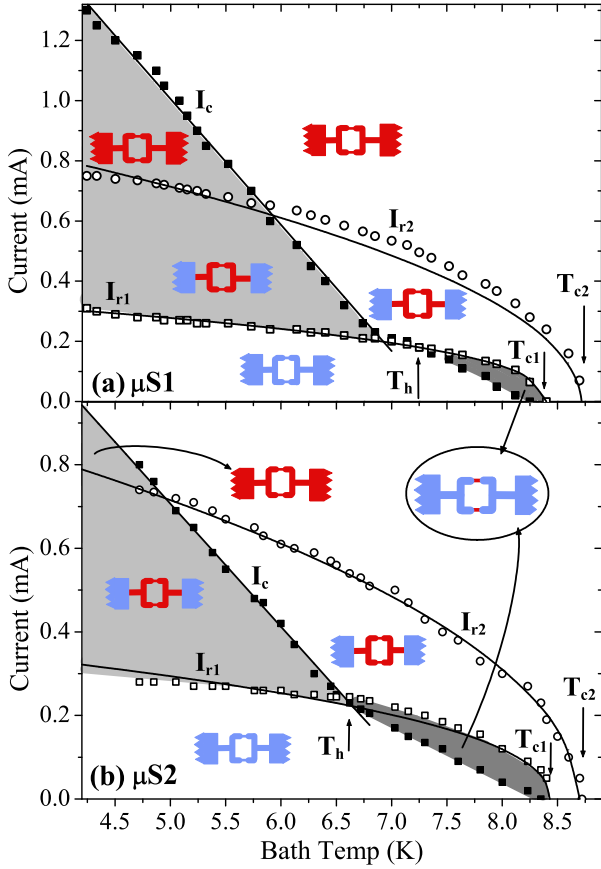


FIG. 4: Variation of I_c , I_{r1} and I_{r2} with bath temperature for (a) μS1 and (b) μS2 . The symbols are the data points. The continuous lines are fits given by (in mA and K), (a) $I_c = 0.42(7.4 - T_b)$ and (b) $I_c = 0.29(7.4 - T_b)$ while the other two are described by $I_{r1} = 0.17(8.4 - T_b)^{0.43}$ and $I_{r2} = 0.37(8.7 - T_b)^{0.5}$ for both the devices. The cartoon pictures of the device shown in different regions depict the state of the device during current ramp-down with blue as SC and red as resistive portions. The light gray-shaded area shows the bistable region where the whole device is in the fully SC state during the current ramp-up from zero. In the dark gray-shaded region, only WLs are resistive.

current bias, we do see the expected voltage oscillations with flux in this regime [18].

Using the long lead approximation for the wide leads, we can fit I_{r2} with Eq. 1 which writes here $I_{r2} = w\sqrt{2\alpha(T_{c2} - T_b)/R_{\square}}$. We obtain a very good fit, see Fig. 4 with the only free parameter being $\alpha = 5.3 \text{ W/cm}^2\cdot\text{K}$, in good agreement with reported values [9, 11]. With the same parameters, except $w = 0.3 \mu\text{m}$, Eq. 1 predicts for the narrow leads a current I_{r1} significantly smaller than observed. This is expected as the presence of wide leads at a short distance makes the heat evacuation more efficient, leading to a higher run-away current.

In a short WL, i.e. with dimensions less than the SC coherence length, we expect, close to its critical temperature, a linear decrease of I_c with temperature so that

$I_c R_{WL} = \beta(T_c - T_b)$ with $\beta = 0.635 \text{ mV/K}$ [3]. From the I_c slope in Fig. 4(a) for μS1 at temperatures below T_h , we find a $R_{WL}/2$ value of 3Ω , which agrees with our earlier findings. In this same regime, the extrapolated critical temperature value of 7.4 K is related to the intrinsic superconductivity of the WLs. Above T_h , the temperature dependence of I_c changes slope and goes down to zero precisely at the critical temperature T_{c1} of the SQUID loop. From this observation, we conclude that the WLs are SC above T_h owing to proximity effect from the adjacent SC with a higher critical temperature.

Finally, we elaborate on how the behavior change of I_c coincides with its crossing with I_{r1} at T_h . Below the crossover temperature T_h , the critical current I_c exceeds the stability (retrapping) current I_{r1} . In this case, a single phase-slip event induced by thermal fluctuations in the WL can cause a thermal runaway [13]. IVCs thus exhibit a sharp voltage jump at I_c , see Fig. 3(a-d). A distribution of I_c values is obtained, since a phase slip-induced transition is stochastic [20]. Above the crossover temperature T_h , the critical current I_c is smaller than the stability (runaway) current I_{r1} , so that no thermal runaway can happen at I_c : the reversible (mono-stable) regime is obtained. Due to phase-slips proliferation near I_c , the transition to the resistive state (at I_c) is then smeared, see Fig. 3(e). The related non-zero dissipation just below I_c also heats some portion of the device above the bath temperature T_b . Assuming that the whole SQUID loop is at nearly uniform temperature, which is justified since the loop size is comparable to l_{th} , we estimate that the power generated just below I_c of 72 nW for $T_b = 7.25 \text{ K}$ brings the SQUID loop to a temperature of about 7.8 K . Because of this and of the fact that the WL region is actually a SC with a lower critical temperature, the temperature dependence of I_c between T_h and T_{c1} cannot be simply described by that of S-N-S WLs [19]. Due to their respective temperature dependence, I_c and I_{r1} are expected to cross at some temperature even if the WL T_c is same as that of adjacent SC. But then the hysteresis-free regime would have existed over a much narrower temperature range. Thus the smaller T_c of the WL and the proximity SC plays crucial role in widening this hysteresis-free temperature range. Finally, SQUID devices with lower I_c or higher I_{r1} values will help widen this temperature range even further.

In conclusion, we present the complete device-state diagram of Nb based μ -SQUIDS. We highlight a non-classical weak link behavior which is understood in the framework of a thermal instability picture. The non-hysteretic high temperature regime of the weak-links is shown to benefit from proximity superconductivity. The present new understanding of the physical mechanisms at the origin of a non-hysteretic behavior is key to further developments in μ -SQUID magneto-sensors for which the suppression of hysteresis represents a key issue.

Samples were fabricated at the platform Nanofab,

CNRS Grenoble and measurements were carried out in IIT Kanpur. AKG thanks University Joseph Fourier for a visiting fellowship. NK acknowledges the financial support from CSIR, India. This work has been financed by the French Research National Agency, ANR-NanoQuartet (ANR12BS1000701) and the CSIR of the govt. of India.

-
- [1] W. Wernsdorfer, Adv. Chem. Phys. **118**, 99 (2001).
 [2] K. Hasselbach, C. Veauvy, D. Mailly, Physica C **332**, 140 (2000).
 [3] K. K. Likharev, Rev. Mod. Phys. **51**, 101 (1979).
 [4] D. Hazra, J. R. Kirtley, and K. Hasselbach, Appl. Phys. Lett. **103**, 093109 (2013).
 [5] M. Tinkham, Introduction to Superconductivity 2nd ed. (Mc Graw-Hill, New York, 1996).
 [6] D. Hazra, Hysteresis in superconducting weak links and micron size superconducting interference devices, PhD thesis, IIT Kanpur (2011).
 [7] Y. Song, J. Appl. Phys. **47**, 2651 (1976); S. Michotte, S. Mátéfi-Tempfli, L. Piraux, D. Y. Vodolazov and F. M. Peeters, Phys. Rev. B **69**, 094512 (2004).
 [8] H. Courtois, M. Meschke, J. T. Peltonen, and J. P. Pekola, Phys. Rev. Lett. **101**, 067002 (2008).
 [9] W. J. Skocpol, M. R. Beasley, and M. Tinkham, J. Appl. Phys. **45**, 4054 (1974).
 [10] M. Tinkham, J. U. Free, C. N. Lau, and N. Markovic, Phys. Rev. B **68**, 134515 (2003).
 [11] D. Hazra, L. M. A. Pascal, H. Courtois, and A. K. Gupta, Phys. Rev. B **82**, 184530 (2010).
 [12] K. S. Ilin, M. Lindgren, M. Currie, A. D. Semenov, G. N. Goltsman, R. Sobolewski, S. I. Cherednichenko and E. M. Gershenzon, Appl. Phys. Lett. **76**, 2752 (2000).
 [13] N. Shah, D. Pekker, and P. M. Goldbart, Phys. Rev. Lett. **101**, 207001 (2008).
 [14] L. Angers, F. Chiodi, G. Montambaux, M. Ferrier, S. Guéron, H. Bouchiat, and J. C. Cuevas, Phys. Rev. B **77**, 165408 (2008).
 [15] S. K. H. Lam and D. L. Tilbrook, Appl. Phys. Lett. **82**, 1078 (2003).
 [16] Nikhil Kumar, T. Fournier, H. Courtois, and Anjan K. Gupta, AIP Conference Proceedings **1591**, 1591 (2014).
 [17] R. F. Broom and E. H. Rhoderick, Brit. J. Appl. Phys. J. Phys. **11**, 292 (1960).
 [18] See the supplementary Information below.
 [19] P. Dubos, H. Courtois, B. Pannetier, F. K. Wilhelm, A. D. Zaikin, and G. Schön, Phys. Rev. B **63**, 064502 (2001).
 [20] T. A. Fulton and L. N. Dunkelberger, Phys. Rev. B **9**, 4760 (1974).

Supplementary Information

SQUID oscillations with magnetic flux

Figure 5 below shows the oscillations in I_c for μS1 at 4.25 K (below T_h) and in voltage at 7.4 K (above T_h) with external magnetic flux. The voltage oscillations are

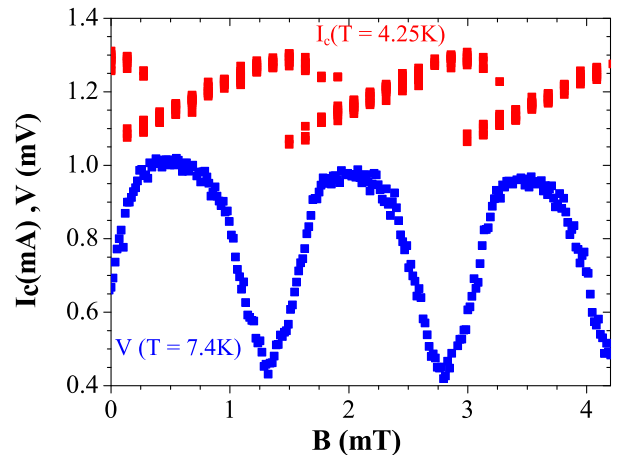


FIG. 5: I_c oscillations in hysteretic regime for μS1 at 4.25K (Red curve) and the voltage oscillations (at 0.17mA current) in non-hysteretic regime at 7.4K (Blue curve).

acquired at a bias current of 0.17 mA, which is close to the critical current at this 7.4 K. The SQUID oscillations with magnetic field are seen only in I_c and not in I_{r1} and I_{r2} . The temperature dependent I_c values have been extracted from these I_c -Vs-B plots at all temperatures by selecting maximum I_c at each temperature. In the non-hysteretic regime I_c was found from the maximum slope of the IVC. This is found to coincide with the current at which the voltage modulation in V-Vs-B peaks. In both cases, the magnetic field periodicity is found to be 1.5 mT, which defines an effective SQUID loop area as $A_{eff} = \frac{\phi_0}{\Delta B} = 1.3\mu\text{m}^2$, which is larger than the actual patterned (internal) area of $1\mu\text{m}^2$.

Heat sharing during resistive fluctuation

In order to elaborate on the sharing of the extra resistive heat, when the differential element becomes normal, by the three interfaces, we also consider two neighboring differential elements of the same length dx as shown in Fig. 2(b) of the main paper. The one on the left (i.e. from $x = -dx$ to $x = 0$) is at temperature $T_c + dT_1$ and the one on the right (i.e. from $x = dx$ to $x = 2dx$) is at temperature $T_c - dT_2$. The left one gives heat $\dot{Q}_0 = \kappa wt \frac{dT_1}{dx}$ to the middle one, which gives heat $\dot{Q}_1 = \kappa wt \frac{dT_2}{dx}$ to the element on right and thus we get,

$$\kappa wt \frac{dT_1}{dx} = \alpha(T_c - T_b)w dx + \kappa wt \frac{dT_2}{dx} \quad (2)$$

When the middle element becomes resistive due to fluctuations its temperature increases to $T_c + dT$. In this

case the above equation gets modified to

$$\begin{aligned} \kappa wt \frac{dT_1 - dT}{dx} &= \alpha(T_c + dT - T_b)wdx \\ &+ \kappa wt \frac{dT_2 + dT}{dx} - I^2 \frac{\rho_n}{wt} dx \end{aligned} \quad (3)$$

Subtracting eq. 2 from eq. 3 we get $2\kappa wt \frac{dT}{dx} = I^2 \frac{\rho_n dx}{wt} - \alpha dT w dx$. Neglecting the higher order second term on the

right, we get $\kappa wt \frac{dT}{dx} = I^2 \frac{\rho_n dx}{2wt}$. Thus the heat current incident from the left interface, i.e. $\dot{Q}'_0 = \kappa wt \frac{dT_1 - dT}{dx} = \dot{Q}_0 - I^2 \frac{\rho_n dx}{2wt}$ and the heat current incident at the right interface, i.e. $\dot{Q}'_1 = \kappa wt \frac{dT_2 + dT}{dx} = \dot{Q}_1 + I^2 \frac{\rho_n dx}{2wt}$. Thus the extra heat generated is equally shared across the two interfaces.